International Journal of Thermal Sciences 165 (2021) 106956

Contents lists available at ScienceDirect

International Journal of Thermal Sciences

journal homepage: http://www.elsevier.com/locate/ijts

Effects of geometric parameters of circular pin-fins on fluid flow and heat transfer in an interrupted microchannel heat sink

Zhenfei Feng [a,b,*], Zhenjun Hu [a], Yongqi Lan [a], Zuqiang Huang [c,**], Jinxin Zhang [d]

[a] School of Mechanical Engineering, Guangxi University, Nanning, 530004, China
[b] Guangxi Key Laboratory of Petrochemical Resource Processing and Process Intensification Technology, Guangxi University, Nanning, 530004, China
[c] School of Chemistry and Chemical Engineering, Guangxi University, Nanning, 530004, China
[d] School of Mechanical and Automotive Engineering, South China University of Technology, Guangzhou, 510641, Guangdong, China

ARTICLE INFO

Keywords:
Microchannel
Numerical simulation
Pin-fins
Heat transfer enhancement
Chaotic advection

ABSTRACT

A novel interrupted microchannel with double circular pin-fins in each microchamber (IMCDCP) is designed to combine the advantages of microchamber and circular pin-fin in heat transfer enhancement. The effects of the diameters (d_1, d_2), spacing (s) and height (h) of circular pin-fin on the local fluid flow and heat transfer characteristics at Reynolds number (Re) of 398 and the average fluid flow and heat transfer characteristics with Re ranging from 133 to 530 in the IMCDCP are investigated using numerical simulation. In addition, to compare with the performance of IMCDCP, the smooth microchannel (SMC), the interrupted microchannel (IMC) and the interrupted microchannel with single circular pin-fin in each microchamber (IMCSCP) are also numerically investigated. These results show that using double circular pin-fins in each microchamber is an effective method in improving heat transfer performance. It effectively reduces the local wall temperature deterioration and achieves better wall temperature uniformity for the interrupted microchannel. The analysis results of geometric parameter show that pin-fin spacing plays an important role in the wall temperature uniformity, and proper pin-fin height is in favor of heat transfer enhancement and pressure drop reduction. The assessment result of overall thermal performance shows optimum geometric parameters for the IMCDCP with $h = 0.08$ mm, $d_1 = d_2 = 0.12$ mm, $s = 0.55$ mm at $Re = 530$, yielding 42% enhancement as compared to SMC.

1. Introduction

With rapid development of electronic devices towards integration, miniaturization and high stability, the thermal management of microelectronic has become a serious challenge to guarantee the long-term reliability and prolong the durable life of electronic devices [1]. Therefore, to solve the problem of high heat flux caused by microelectronic devices, Tuckerman and Pease [2] proposed the concept of microchannel heat sink (MCHS) in 1981. Since then, the MCHS has been commonly used in high heat flux cooling devices due to the advantages of higher heat transfer coefficient, lesser weight and compact structure [3]. However, with continuous advancement of science and technology, the heat dissipation capacities of modern microelectronic devices are close to or exceed 10^6 W/m^2 [4]. Thus, the conventional microchannel heat sink is not enough to remove very high heat flux due to thermal boundary layer thickness. For this reason, it is urgent to improve heat transfer performance of microchannel heat sink to solve cooling problem.

Previous studies have proved that heat transfer performance of microchannel heat sink can be effectively enhanced by changing internal structure or using enhanced working fluid, such as changing channel shapes [5], adding cavities or secondary channels [6] and ribs/pin-fins [7], as well as using nanofluids [8]. In terms of nanofluids as working fluids in microchannels, many studies have indicated that adding low volume fraction of nanoparticles to the coolant can significantly improve thermal conductivity of the coolant [9–11]. Thus, the use of nanofluid has a positive improvement in heat transfer as compared to base fluids [12,13]. However, using nanofluid in the cooling system may reduce the system stability due to aggregation and sedimentation of nanoparticles. This limits the application of nanofluids in the cooling system [14]. Furthermore, Khoshvaght-Aliabadi et al. [15] concluded in their study that using an enhanced surface was more useful than using enhanced working fluid. Therefore, many scholars are focusing on

* Corresponding author. School of Mechanical Engineering, Guangxi University, Nanning, 530004, China.
** Corresponding author. School of Chemistry and Chemical Engineering, Guangxi University, Nanning, 530004, China.
E-mail addresses: zffeng@gxu.edu.cn (Z. Feng), huangzq@gxu.edu.cn (Z. Huang).

https://doi.org/10.1016/j.ijthermalsci.2021.106956
Received 2 October 2020; Received in revised form 18 February 2021; Accepted 9 March 2021
Available online 30 March 2021

Nomenclature

A	area, m^2
c_p	specific heat capacity, J/(kg·K)
d	circular pin-fin diameter, mm
D_h	hydraulic diameter, mm
f	friction factor
h	pin-fin height, mm
h_{ave}	average heat transfer coefficient, $W/(m^2 \cdot K)$
H_{ch}	microchannel height, mm
L	microchannel length, mm
Nu	Nusselt number
p	pressure, Pa
Δp	pressure drop, Pa
P_x	local pressure, Pa
q	heat flux, W/m^2
Re	Reynolds number
s	pin-fin spacing, mm
T	temperature, K
$\boldsymbol{U}$	velocity vector
u, v, w	velocity components in the x, y, z direction, m/s
V	volume, m^3
W_{ch}	microchannel width, mm
x/L	non-dimensional length
x, y, z	three coordinates shown in Fig. 1, mm

Greek symbols

λ	thermal conductivity, W/(m·K)
ρ	density, kg/m^3
μ	dynamic viscosity, Pa·s

Subscripts

ave	average
ch	channel
D	Darcy
in	inlet
f	fluid
out	outlet
s	solid
w	wall
x	x direction
0	smooth microchannel

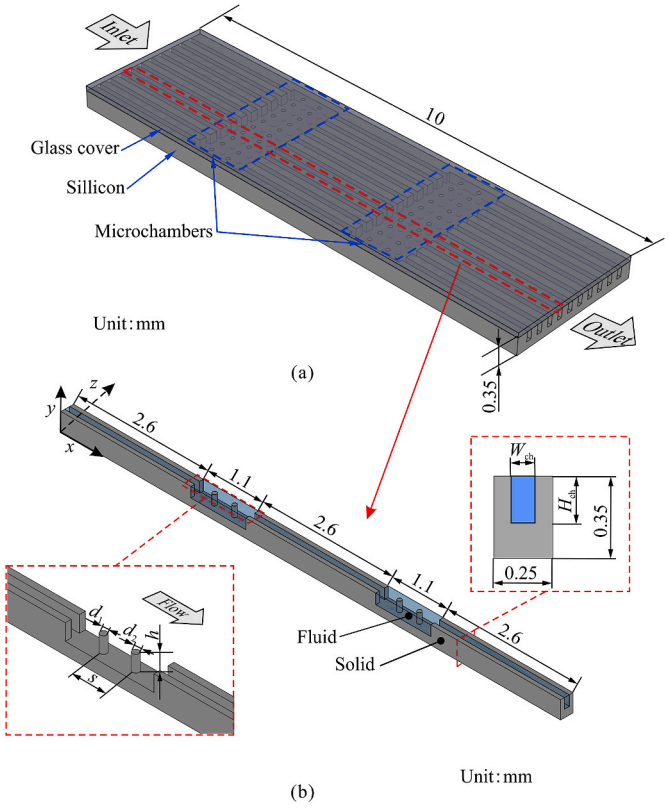

Fig. 1. Schematic diagrams of (a) an interrupted microchannel heat sink and (b) a single microchannel.

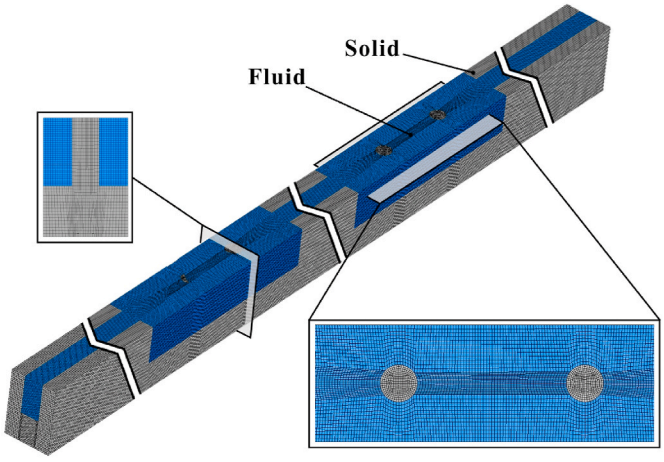

Fig. 2. Grids of IMCDCP with $d_1 = d_2 = 0.8$ mm, $h = 0.2$ mm and $s = 0.4$ mm.

surface enhancement of microchannel.

For microchannel heat sink with cavities or secondary channels, heat transfer enhancement could be attributed to the spurting and throttling effects, as well as the interruption and redevelopment of the hydraulic and thermal boundary layers [16,17]. Wan et al. [18] performed an experiment to study flow characteristics and heat transfer performance of half-corrugated microchannels. They observed that the pressure drop was significantly reduced by the presence of cavities at the given Reynolds number, and the heat transfer performance was enhanced when the heat flux was beyond 150 kW/m^2. Yuan et al. [19] carried out the experimental and numerical study on the heat transfer and flow characteristics in the non-uniform wavy microchannels. The results showed that the divergent wavy microchannel had better heat transfer performance than the uniform microchannel and convergent wavy microchannel at Reynolds number ranging from 177 to 822. Liu et al. [20] used serpentine microchannel with fan-shaped reentrant cavities in their numerical study and observed that the fan-shaped cavities was able to effectively reduce the flow resistance and improve the temperature distribution uniformity. Raja Kuppusamy et al. [21] carried out a numerical study for thermal enhancement in microchannel heat sink with secondary flow. They found that the thermal performance increased with the width and number of secondary channel increasing. Moreover, the reduction in the angle of the secondary flow path easily rendered the fluid to be transferred to the secondary flow path, thereby enhancing heat transfer. Shi et al. [22] and Yang and Cao [23] investigated the microchannel heat sink with secondary flow channel to find the optimization of geometry parameters on heat transfer and fluid flow

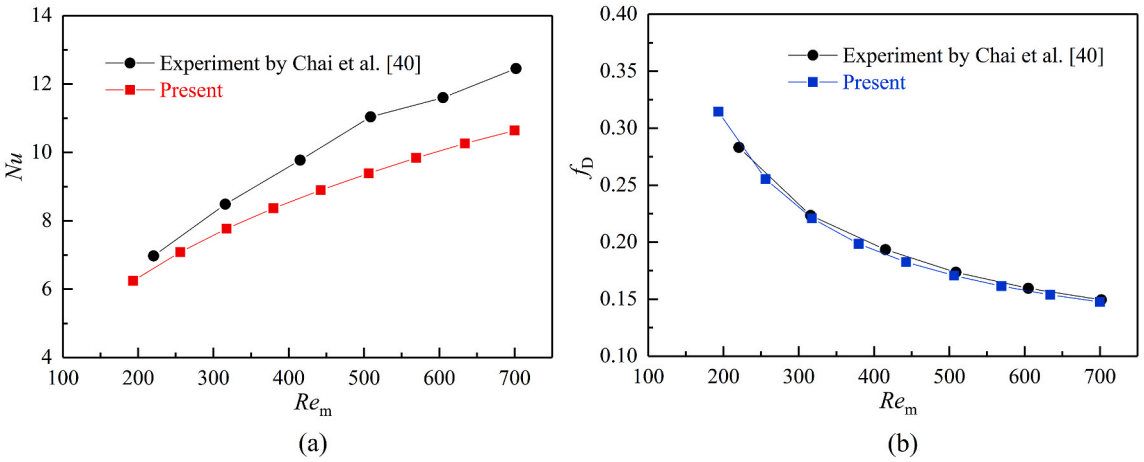

Fig. 3. Comparison between results of present model and Chai et al. [40] for (a) Nu and (b) f_D.

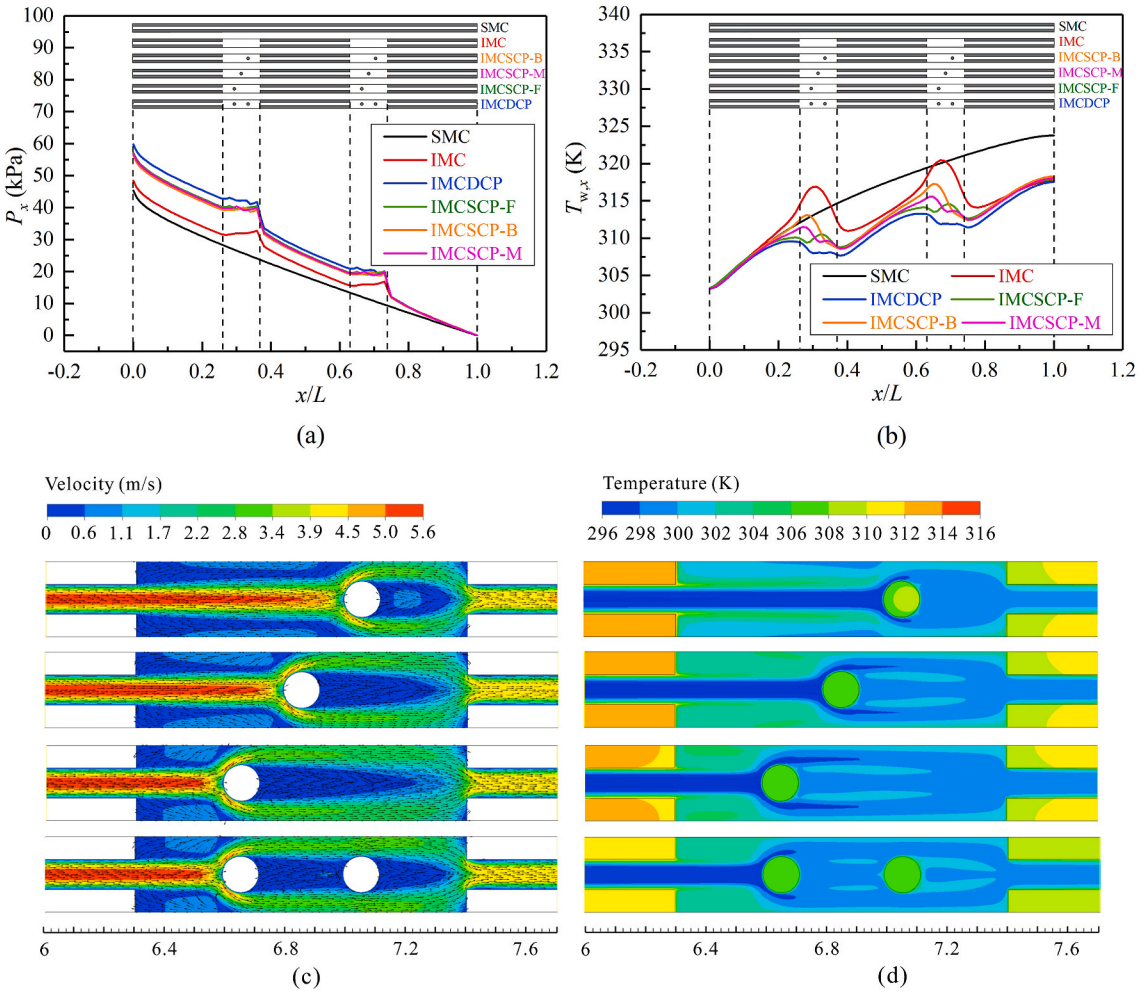

Fig. 4. Effects of different microchannel structures on (a) local pressure and (b) local wall temperature. Distributions of (c) velocity and (d) temperature in the plane at y = 0.25 mm with x = 6.0–7.7 mm for Re = 398.

characteristics.

For the microchannel heat sink with ribs/pin-fins, heat transfer is improved significantly, albeit with a higher pressure drop penalty [24]. Prajapati [25] numerically investigated heat transfer and fluid flow characteristics in rectangular microchannel heat sink with different pin-fin heights. They found that the heat transfer performance increased at first and then decreased with the increase in pin-fin height. Wang et al. [26] numerically and experimentally examined the fluid and heat transfer characteristics in the microchannel heat sink with truncated rib on sidewall. Li et al. [27] carried out an experimental study on the heat transfer and flow characteristics in the microchannels with micro-ribs. They observed that the heat transfer enhancement could be attributed

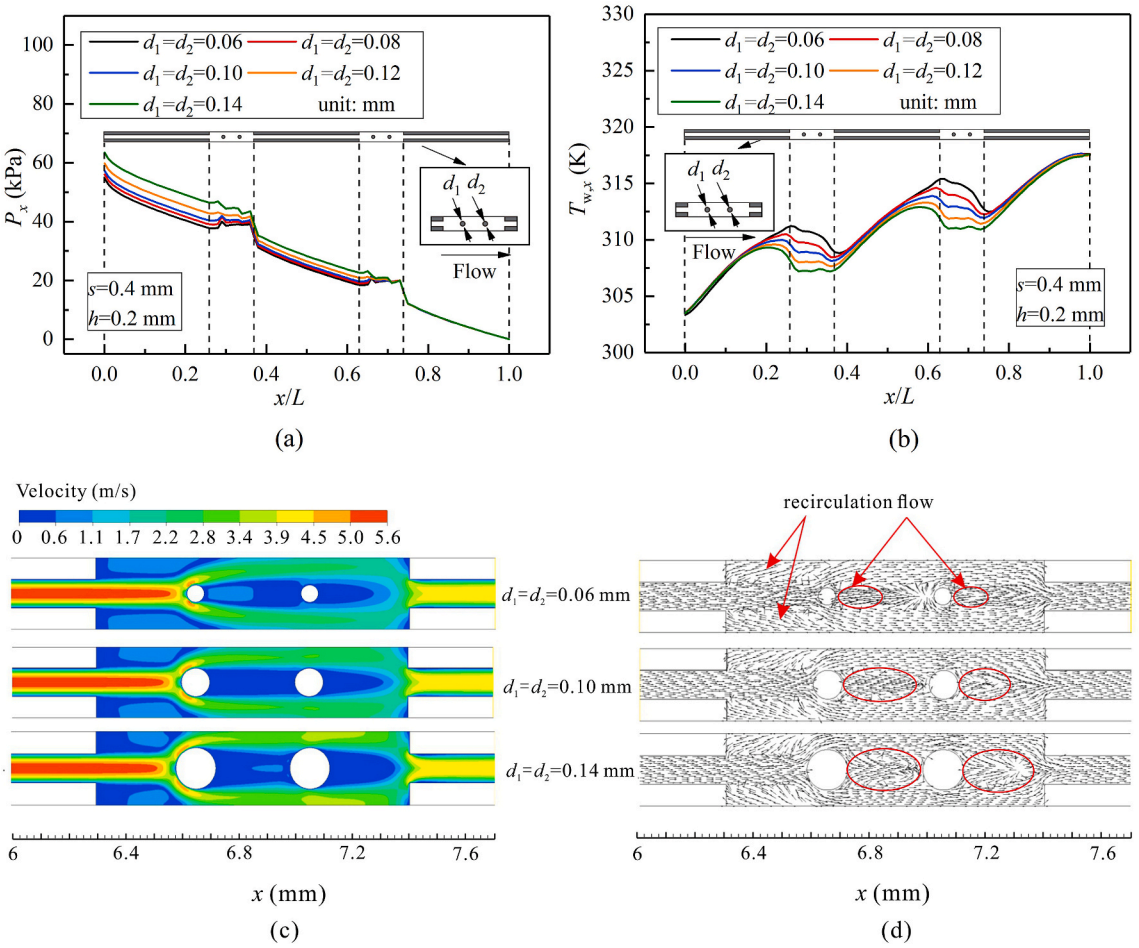

Fig. 5. Effects of different pin-fin diameters on (a) local pressure and (b) local wall temperature. Distributions of (c) velocity field and (d) velocity vector in the plane at y = 0.25 mm with x = 6.0–7.7 mm for Re = 398.

to the recirculation, as well as the jetting and throttling effects due to the presence of ribs. Jia et al. [28] used combined microchannel with cone-shaped micro-pin-fins in their numerical study and presented that pin-fins were beneficial to enhance the heat transfer but accompanied with a higher pressure drop. Wang et al. [29] proposed the mini-channel with discrete double-inclined ribs for improving the heat transfer. They found that strong longitudinal vortex was generated in near the tips of each rib, which enhanced heat transfer effectively. Hosseinirad et al. [30] studied the heat transfer and pressure drop of the transverse rectangular vortex-generators with various non-uniform heights in a mini-channel. Ma et al. [31] investigated the heat transfer and fluid flow characteristics of the microchannel heat sink with periodic jetting and throttling structures in sidewalls. Wang et al. [32] carried out a study on the microchannel heat sink with bidirectional ribs which composed of vertical rib and spanwise rib. The results showed that heat transfer performance of the complex combined bidirectional ribs was better than that of vertical ribs or spanwise ribs, but it also gave rise to the larger pressure drop penalty.

For the microchannel heat sink with combination of ribs/pin-fins and cavities (or secondary channels), Japar et al. [33] numerically studied the combination of ribs and secondary channels and observed that ribs contributed to eliminating the stagnation zone by guiding fluid flow toward the cavities zone, thereby enhancing heat transfer. Ghani et al. [34] performed a numerical study on the microchannel with combination of cavities and ribs. They found that it had more superior overall thermal performance than using individual technique. Li et al. [35] compared microchannel heat sink having triangular cavities and ribs with microchannel heat sink having triangular cavities. The results showed that the combination of triangular cavities and ribs had better heat transfer performance than microchannel with triangular cavities. Ghani et al. [36] carried out a numerical study on the microchannel heat sink with ribs and secondary channels. They found that the heat transfer was significantly enhanced due to removing the stagnation zone in secondary channel and promoting flow mixing between the adjacent main channels. Moreover, the pressure drop penalty caused by ribs would be reduced thanks to the presence of secondary channels. Datta et al. [37] used their numerical results to find the best performance for rectangular microchannel with trapezoidal cavities and ribs. A and Chakraborty [38] investigated the microchannel with circular pin-fins and micro blind holes. They observed that circular pin-fins improved the heat transfer while the micro blind holes decreased pressure drop.

Based on the above literature review, it is found that the ribs/pin-fins effectively improve heat transfer and cavities (or secondary channels) are beneficial to reduce the pressure drop, to a certain extent. The combination of ribs/pin-fins and cavities (or secondary channels) provides superior performance because it combine the advantages of ribs/pin-fins and cavities (or secondary channels). Also, it is worth noting that the secondary channels formed by slotting the channel wall between adjacent channels is conducive to reduce pressure drop, due to the enlargement of flow area [21–23,36]. According to this method, Alfellag el al. [39] experimentally studied slotted oval pins in trapezoidal cavities and observed that slotted oval pins in cavities effectively improved overall thermal performance. This implies that slotted pin-fins is an effective method to obtain better performance. Additionally, it is also found that numerous studies focus on the microchannel with the combination of single rib/pin-fin and single cavity (or secondary channel),

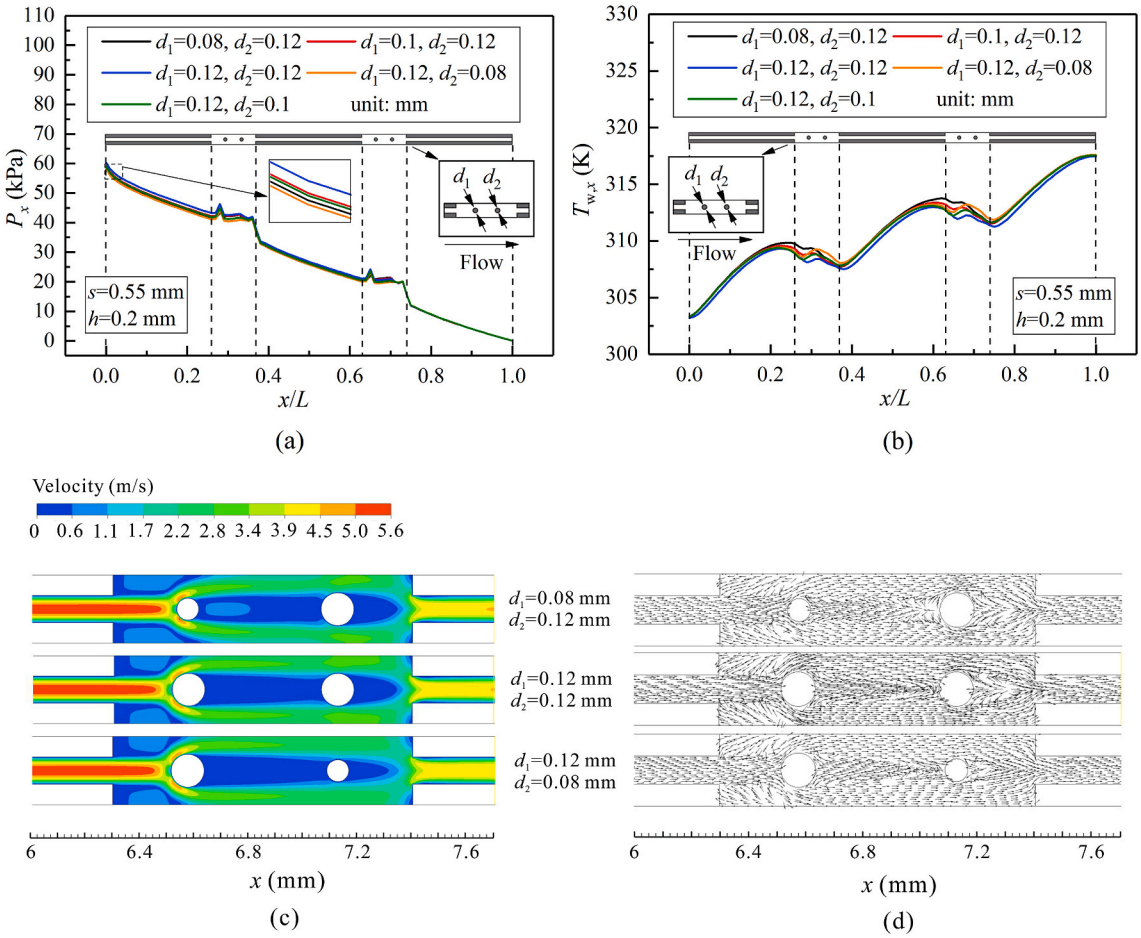

Fig. 6. Effects of combination of different pin-fin diameters on (a) local pressure and (b) local wall temperature. Distributions of (c) velocity field and (d) velocity vector in the plane at y = 0.25 mm with x = 6.0–7.7 mm for Re = 398.

and the microchannel with the combination of multi-ribs/pin-fins and single cavity (or secondary channel) is neglected. Thus, a microchannel with combination of the double circular pin-fins (similar to slotted pin-fin) and microchamber (similar to the big secondary channel) is designed in present work, based on the work conducted by Chai et al. [40]. This design is beneficial to provide larger flow area to reduce pressure drop as compared to the long rib in microchamber. Moreover, the double circular pin-fins are also helpful to inducing more formation of vortex and promoting the mixing of hot and cold fluid. To understand the effects of geometric parameters on fluid flow and heat transfer in this novel microchannel, the diameters of pin-fins in upstream and downstream of microchamber, the spacing between double circular pin-fins and the height of pin-fin are selected as geometric parameters. Also, the effects of these geometric parameters on the local pressure, local wall temperature, average flow and heat transfer characteristics in the novel microchannel are analyzed.

2. Numerical simulation

2.1. Physical model

Fig. 1(a) displays the schematic view of interrupted microchannel heat sink with circular pin-fins in this study. There are two microchambers in the microchannel heat sink and the circular pin-fins are arranged in each microchamber. The glass cover is bonded to the microchannel heat sink to form the enclosed passages. To save computational cost for this simulation and considering the repeatability of microchannels heat sink, the symmetry condition is used for the microchannel heat sink model. Thus, a single interrupted microchannel and its nearby solid sections are selected in present numerical study. Fig. 1(b) shows the computational domain of an interrupted microchannel with double circular pin-fins in each microchamber (IMCDCP). The height (H_{ch}) and width (W_{ch}) of microchannel are 0.2 mm and 0.1 mm, respectively. To understand the impacts of the geometric parameters of double circular pin-fins on the fluid flow and heat transfer in the interrupted microchannel, the diameter (d_1) of pin-fin in upstream of microchamber, the diameter (d_2) of pin-fin in downstream of microchamber, the spacing (s) between double circular pin-fins, and the height (h) of circular pin-fin are selected as studied parameters. They are in ranges of 0.06–0.14 mm, 0.06–0.14 mm, 0.25–0.85 mm and 0.04–0.2 mm, respectively. More details about geometric parameters of IMCDCP are presented in Fig. 1(b).

2.2. Numerical model

In this simulation, silicon is selected as the material of the solid domain and the working fluid is water. To simplify this numerical model, several assumptions are made as follows:

(1) Flow is Newtonian, steady and continuous incompressible laminar flow.
(2) Volume force, surface tension and radiation heat transfer are neglected.
(3) Varied thermophysical properties of working fluid are employed and the data is shown in the Ref. [40].
(4) Thermophysical properties are constant for the solid domain.

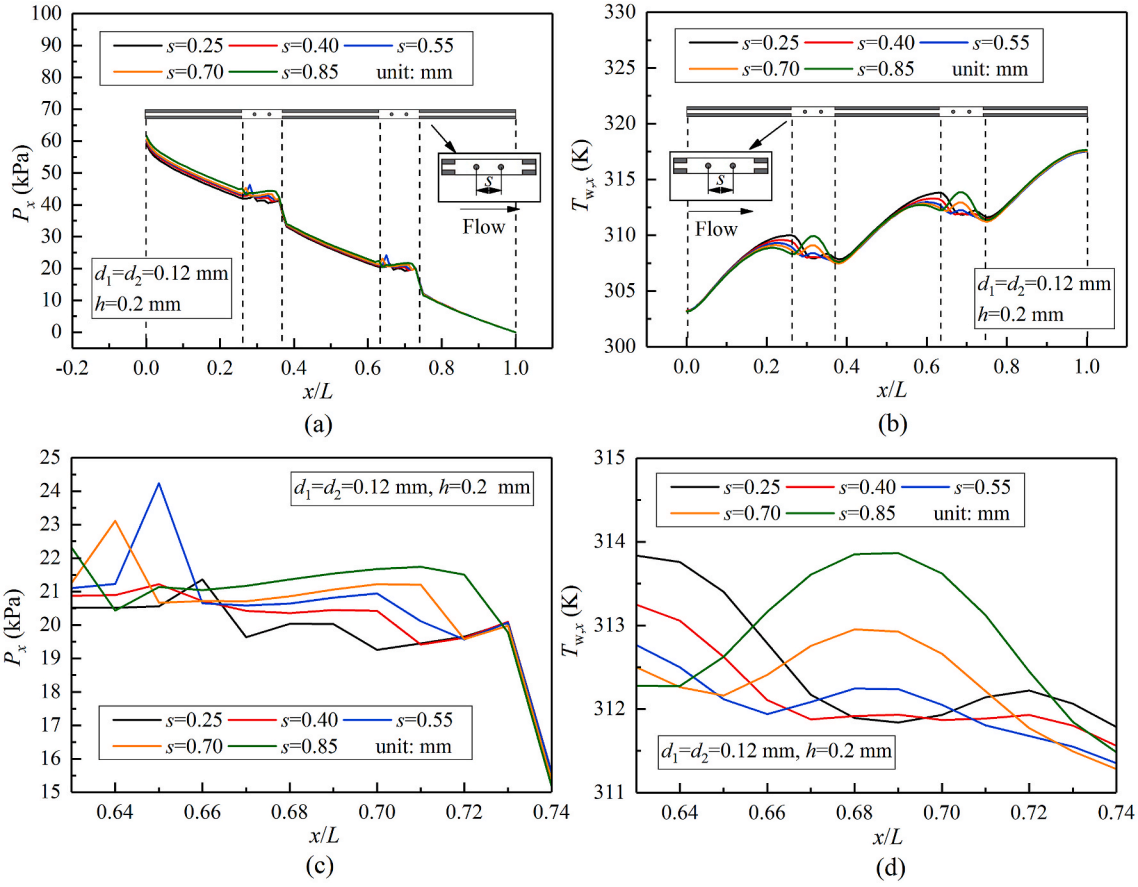

Fig. 7. Effects of different pin-fin spacings on (a) local pressure and (b) local wall temperature. Enlarged views of (c) local pressure and (d) local wall temperature at $0.63 < x/L < 0.74$.

Based on above simplifying assumptions, the continuous equation, momentum equation and energy equation for fluid domain can be obtained as:

$$\nabla\cdot(\rho \boldsymbol{U}) = 0 \tag{1}$$

$$\nabla\cdot(\rho \boldsymbol{U}\boldsymbol{U}) = -\nabla p + \nabla(\mu\nabla \boldsymbol{U}) \tag{2}$$

$$\nabla\cdot\left(\rho c_p \boldsymbol{U} T_f\right) = \nabla\cdot\left(\lambda_f \nabla T_f\right) \tag{3}$$

For solid domain, the energy equation is expressed as:

$$\lambda_s \nabla^2 T_s = 0 \tag{4}$$

where p, ρ, μ, c_p, λ_f and T_f are the pressure, density, viscosity, specific heat capacity, thermal conductivity, and temperature of the fluid, respectively. λ_s and T_s are the thermal conductivity and temperature of the solid, respectively.

In this simulation, the uniform velocity (u_{in} = 1–4 m/s) and constant temperature (T_{in} = 293 K) are employed at the inlet of microchannel. The average static pressure boundary condition is specified with a fixed pressure of 0 Pa (relative to the environment) at the outlet of microchannel. A constant heat flux of $q = 10^6$ W/m^2 is applied on the base wall of microchannel. The solid walls coupled with fluid are set as the fluid-solid interface boundary conditions. A symmetry boundary condition is applied on two sides of the computational domain. Adiabatic wall boundary conditions are assigned for other walls. Computational Fluid Dynamics (CFD) software CFX is used to solve the above control equations. When the convergence residual is less than 10^{-5}, the numerical solutions are considered to be converged.

2.3. Grid independence

The accuracy of the numerical simulation results is generally determined by the quality and size of the grids. Thus, the structural grid is used for the numerical simulation. Furthermore, to eliminate the error caused by coarseness of grids, the independent verification of grid size has been carried out prior to detailed analysis. For example, the grid number of IMCDCP with $d_1 = d_2 = 0.8$ mm, $h = 0.2$ mm and $s = 0.4$ mm is varied by 1.7805 million, 2.7154 million and 3.5889 million. According to the simulation results at inlet velocity of 2 m/s, the relative errors of pressure drop using 1.7805 and 2.7154 million grids from that using 3.5889 million grids are 2.02% and 0.69%, respectively. This means that the IMCDCP with $d_1 = d_2 = 0.8$ mm, $h = 0.2$ mm and $s = 0.4$ mm using 2.7154 million grids can obtain numerical results with enough accuracy. Thus, the grid system with 2.7154 million grids is selected for numerical simulation in present study. The final meshing of this microchannel is shown in Fig. 2.

2.4. Data reduction

The Reynolds number (Re) based on inlet parameters is expressed as:

$$Re = \frac{\rho_{in} u_{in} D_h}{\mu_{in}} \tag{5}$$

where ρ_{in}, μ_{in} are the density and viscosity of fluid at inlet, respectively; D_h is the hydraulic diameter and is defined as:

$$D_h = \frac{2W_{ch}H_{ch}}{W_{ch} + H_{ch}} \tag{6}$$

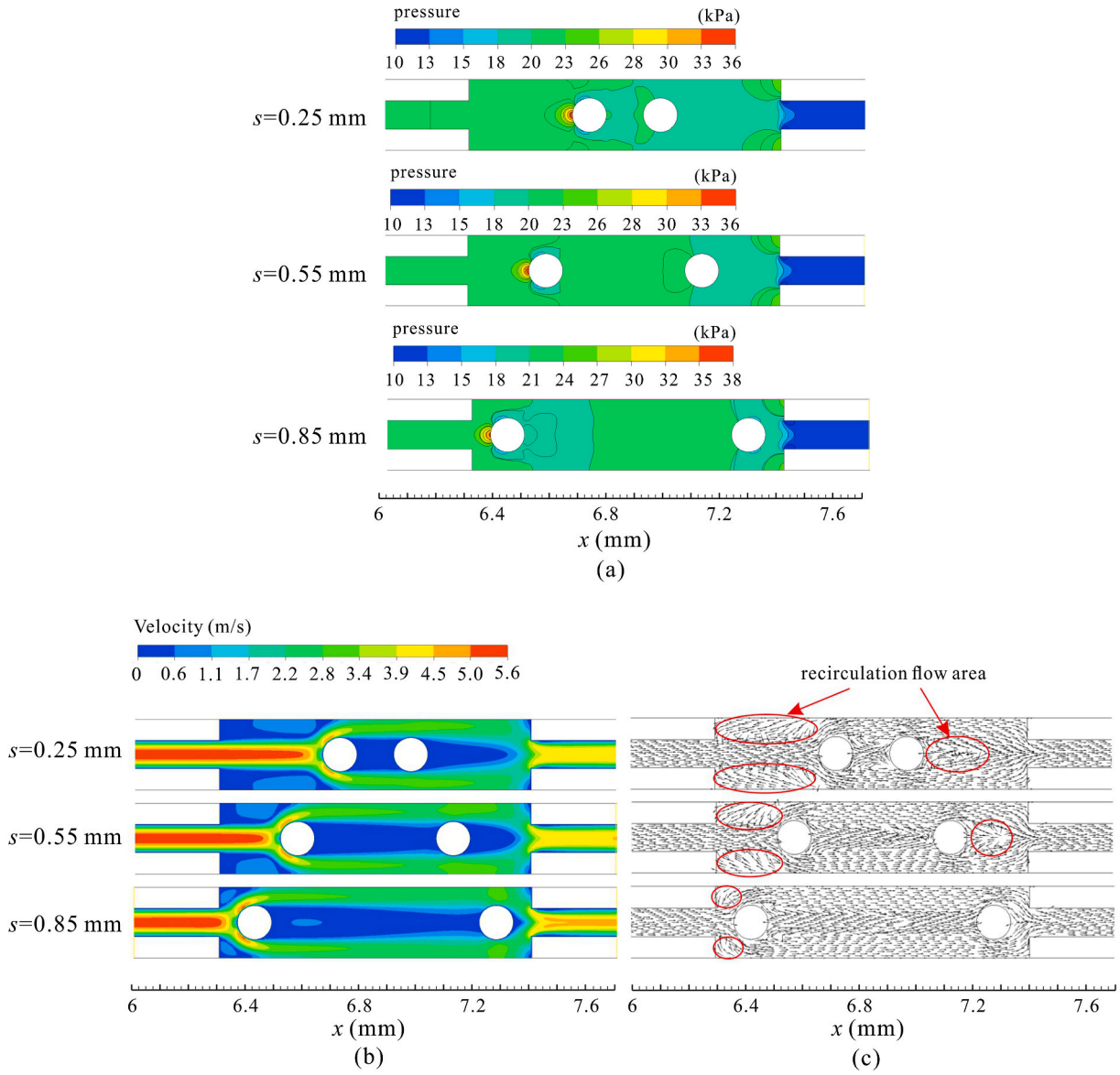

Fig. 8. Distributions of (a) pressure field, (b) velocity field and (c) velocity vector for different pin-fin spacings in the plane at $y = 0.25$ mm with $x = 6.0$–7.7 mm for $Re = 398$.

Where W_{ch} and H_{ch} are the width and height of single microchannel, respectively.

The local pressure (P_x) of fluid in microchannel is calculated from:

$$P_x = \frac{\int p_{x,i}\rho_i \left|\vec{u}\cdot d\vec{A}\right|}{\int \rho_i \left|\vec{u}\cdot d\vec{A}\right|} \tag{7}$$

The local temperature ($T_{w,x}$) of heat sink bottom wall is obtained from:

$$T_{w,x} = \frac{\int T_{w,i} dz}{\int dz} \tag{8}$$

The average Fanning friction factor (f) of the microchannel is estimated from:

$$f = \frac{\Delta p D_h}{2\rho_m u_{in}^2 L} \tag{9}$$

where Δp is pressure drop of the microchannel; L is length of microchannel; ρ_m is the volume average density of fluid.

The average Nusselt number (Nu) is given by:

$$Nu = \frac{h_{ave} D_h}{\lambda_m} \tag{10}$$

where λ_m is the mass average thermal conductivity of fluid; h_{ave} is the average heat transfer coefficient, which is calculated by:

$$h_{ave} = \frac{qA_w}{A_{sf}\left[T_{w,ave} - 0.5(T_{out} + T_{in})\right]} \tag{11}$$

where A_w, A_{sf}, $T_{w,ave}$ and T_{out} are the heating area, convection heat transfer area, average temperature of the silicon base and average fluid temperature at the outlet, respectively.

To compare the thermal and hydrodynamical performances of the interrupted microchannels having different pin-fin parameters with these of the smooth microchannel, the performance evaluation criterion factor (*PEC*) is studied as a measure of the amount of the heat transfer enhancement coefficient against the friction factor increase, and is defined as:

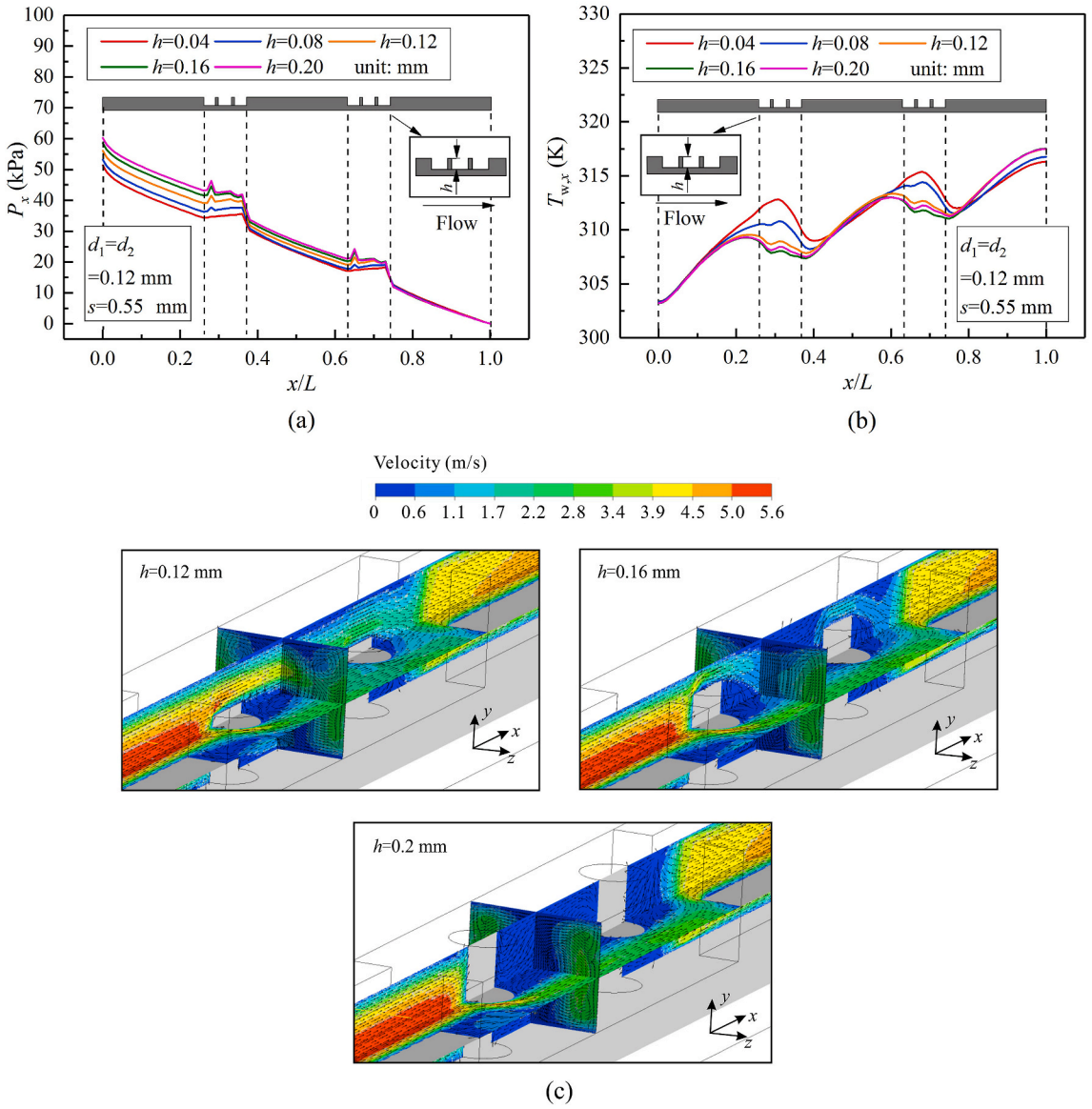

Fig. 9. Effects of different pin-fin heights on (a) local pressure, (b) local wall temperature, and (c) velocity field and velocity vector for $Re = 398$.

$$PEC = \frac{Nu/Nu_0}{(f/f_0)^{1/3}} \tag{12}$$

where Nu_0 and f_0 represent the Nusselt number and friction factor of the smooth microchannel, respectively.

3. Results and discussion

3.1. Validation with experimental data

To verify the accuracy and reliability of the present numerical method, the numerical results for the interrupted microchannel with rectangular ribs is compared with the experimental results by Chai et al. [40]. In their experiment, a constant heat flux of 1.22×10^6 W/m^2 is applied at the base wall of microchannel. Fig. 3 shows that the Nusselt number (Nu) and Darcy friction factor (f_D) for the present numerical simulation are validated with the experimental value. In this figure, the Reynolds number (Re_m) is calculated on the basis of the fluid properties at the arithmetic mean temperature of the microchannel inlet and outlet, which is the same as in experiment by Chai et al. [40]. It is clearly seen that the numerical results are in good agreement with the experimental data at all given Re_m. The maximum relative errors between numerical and experimental results for the Nusselt number and friction factor are less than 14.5% and 6.5%, respectively. This indicates that the present numerical method can validly predict the fluid flow and heat transfer characteristics in the present numerical simulation.

3.2. Local flow and heat transfer performance

3.2.1. Effects of microchannel structure

It is well known that the interruption and development of the thermal boundary layer, as well as the generation of vortex and chaotic advection are helpful to improving the heat transfer performance in the microchannel. Thus, the purpose of adding double circular pin-fins in each microchamber of an interrupted microchannel is to induce more vortex formation and to promote chaotic advection, thereby enhancing heat transfer. In practice, the pressure drop and the base wall temperature are two key indicators in electronic devices application. Lower pressure drop means lower pumping power, as well as lower wall temperature and better wall temperature uniformity are beneficial to the stability of electronic devices. Fig. 4(a) and (b) present the variations of local pressure (P_x) and local wall temperature ($T_{w,x}$) with the non-

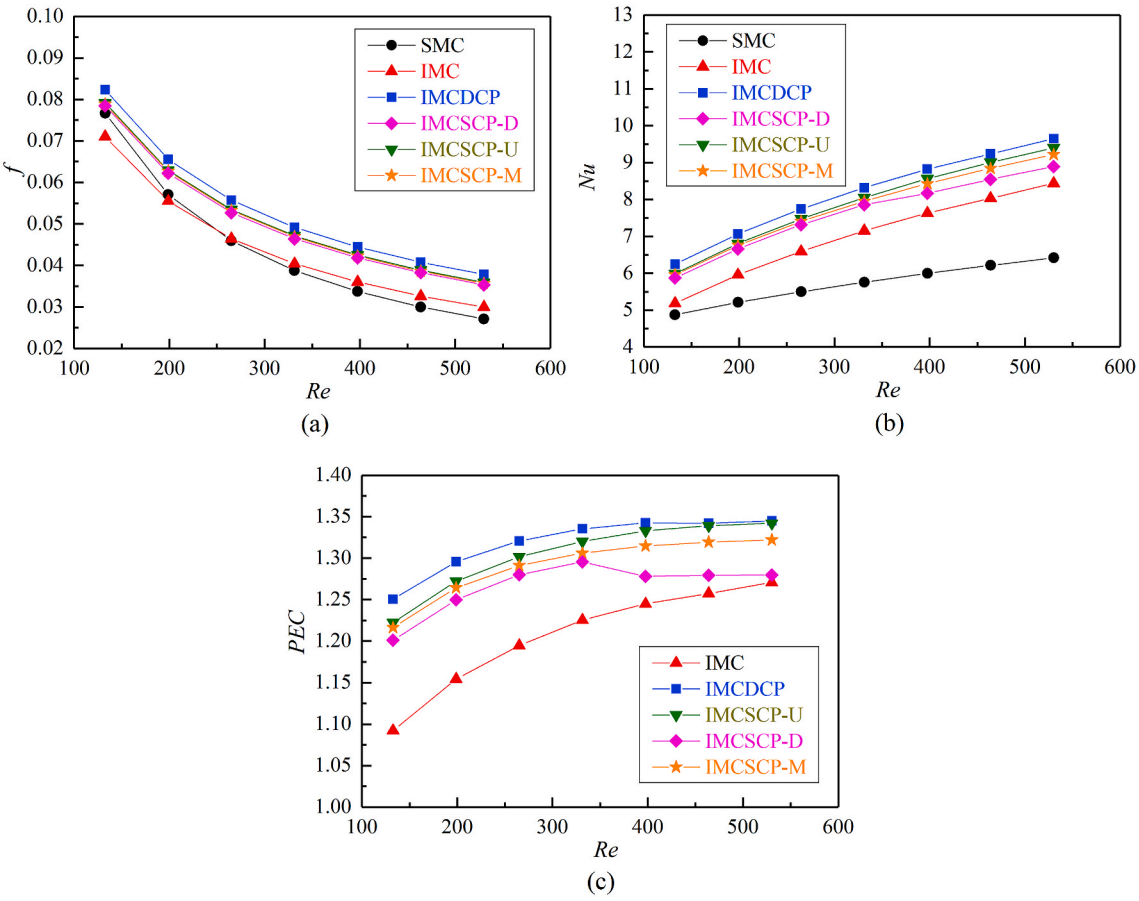

Fig. 10. Variations of (a) *f*, (b) *Nu* and (c) *PEC* with *Re*.

dimensional length (x/L) at $Re = 398$ for six configurations, including a smooth microchannel (SMC), an interrupted microchannel (IMC), three interrupted microchannels with single circular pin-fin in each microchamber (IMCSCP) and an interrupted microchannel with double circular pin-fins in each microchamber (IMCDCP). For the IMCSCP, three pin-fin positions in microchamber are examined, and they are named as IMCSCP-U (pin-fin in upstream), IMCSCP-M (pin-fin in midstream) and IMCSCP-D (pin-fin in downstream), as shown in Fig. 4(a) and (b). From Fig. 4(a), it is obviously noticed that the local pressure of SMC decreases gradually with x/L due to the friction loss. The local pressures of IMC, IMCSCP and IMCDCP also present similar trends along the microchannel except the microchamber where pressure fluctuation occurs. In the microchamber of IMC, the local pressure along flow direction increases slightly and then decreases rapidly before the fluid flows into microchannel. This is because the cross-sectional area of fluid flow in microchamber is larger than that in microchannel, resulting in a decrease of fluid velocity when the fluid flows from microchannel into the microchamber. Thus, according to the Bernouli law, the pressure will increase. However, due to the flow resistance existing in the microchamber, the pressure increases slightly along the flow direction. In addition, before the fluid flows from the microchamber into the microchannel, the fluid is blocked by the long ribs between two adjacent microchannels, causing a large pressure loss. When the fluid flows into the microchannel, the velocity will increase and the pressure will decrease due to the small cross-sectional area of the microchannel. These behaviors render the pressure to decrease rapidly during which the fluid flows from microchamber into microchannel. In the microchambers of IMCSCP and IMCDCP, the local pressure along flow direction decreases slightly and wavily. This can be attributed to the flow blockage effect caused by circular pin-fin in the microchamber. This effect brings more flow resistances in the microchamber with double pin-fins. Thus, the IMCDCP achieves the highest pressure drop, and the SMC yields the lowest pressure drop.

In Fig. 4(b), the local temperature of IMC shows the highest value in microchamber as compared to other microchannels. This is because low fluid velocity in the microchamber of IMC results in thick boundary layer, thereby increasing thermal resistance. For IMCSCP and IMCDCP, the pin-fin mounted in microchamber not only increases the heat transfer area of the microchannel, but also promotes the fluid disturbance. Hence the wall temperature is greatly reduced as compared to IMC. This indicates that the pin fin in the microchamber plays an important role in the local temperature. Additionally, the interrupted microchannel with pin-fin in the upstream of microchamber (IMCSCP-U) has lower wall temperature than that in the midstream (IMCSCP-M) or downstream (IMCSCP-D). This is because the pin-fin in the upstream of the microchamber is impacted by high flow velocity, inducing higher turbulence intensity in the flow and helping to develop the vortex behind the pin-fin. It is worth noting that the IMCDCP has lower local temperature and better wall temperature uniformity than all IMCSCPs. This can be attributed to the fact that the double circular pin-fins not only increases heat transfer area and makes higher turbulence intensity, but also improves insufficient flow disturbance caused by single pin-fin. In general, the combination of double circular pin-fins and microchamber can reduce the local wall temperature and improve the wall temperature uniformity, which is significant for the temperature rise of the heat sink base along the flow direction. This means that the IMCDCP is invaluable for applications involving hot spots mitigation in the electronic devices.

To understand the effect of circular pin-fin in the microchamber on heat transfer enhancement, it is necessary to analyze the velocity and

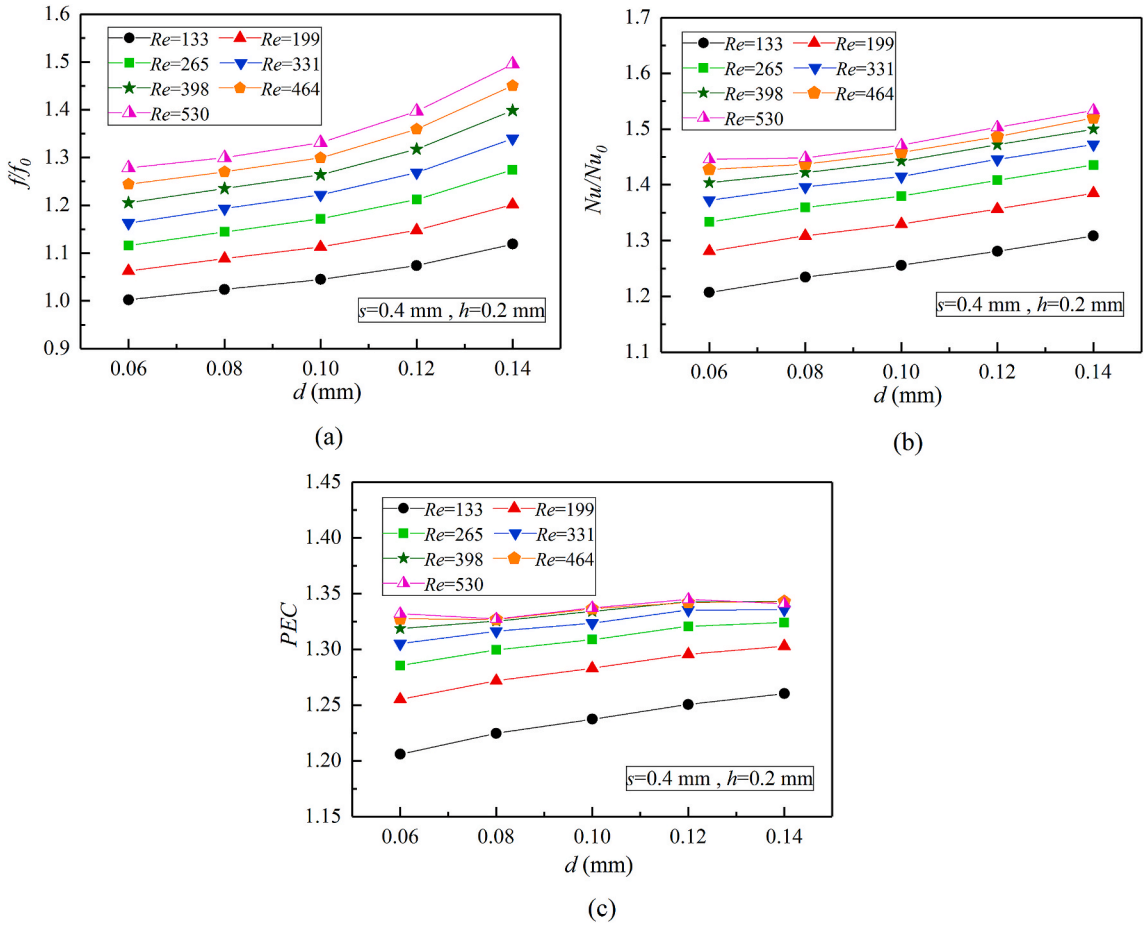

Fig. 11. Variations of (a) f/f_0, (b) Nu/Nu_0 and (c) *PEC* with pin-fin diameter for different Reynolds numbers.

temperature distributions in the microchamber of the interrupted microchannel with circular pin-fin. Fig. 4(c) and (d) show the distributions of velocity and temperature in the plane at $y = 0.25$ mm with $x =$ 6.0–7.7 mm for $Re = 398$. It can be observed that the fluid velocity is redistributed due to the existence of microchamber and circular pin-fin. For different positions of single pin-fin, the pin-fin in the upstream is impacted by more fluid with high flow velocity as compared to the pin-fin in the midstream or downstream. This brings higher turbulence intensity and promotes the development of vortex behind the pin-fin, rendering the flow boundary layer to reduce further. For double circular pin-fins, more vortexes are generated, and the vortex intensity further enhances as compared to single pin-fin. This further promotes fluid mixing and disturbance of the flow boundary layer. In terms of temperature distribution, it is clearly seen from Fig. 4(d) that the thermal boundary layer is interrupted and redeveloped due to the presence of microchamber and pin-fin. For single pin-fin, the pin-fin in the upstream yields lower temperature and better wall temperature uniformity as compared to the pin-fin in the midstream or downstream. However, it is also found that the double circular pin-fins has lower temperature and better wall temperature uniformity as compared to the single pin-fin. Overall, comparing with other microchannels (SMC, IMC and IMCSCP), the IMCDCP significantly improves chaotic advection, as well as induces the better fluid mixing between the mainstream and recirculation flow regions, thereby promoting heat transfer, as well as achieving low level and good uniformity for wall temperature.

3.2.2. *Effects of circular pin-fin diameter for IMCDCP*

According to the above results, it can be concluded that the IMCDCP accomplished the highest local thermal performance as compared to other microchannels. To further improve the overall thermal performance of IMCDCP, it is necessary to analyze the effects of the geometric parameters of double circular pin-fins with different diameters (d_1, d_2), spacings (s) and heights (h) on local fluid flow and heat transfer characteristics.

Fig. 5(a) and (b) illustrate the effects of different circular pin-fin diameters ($d_1 = d_2 =$ 0.08–0.14 mm) on local pressure (P_x) and local wall temperature ($T_{w,x}$) with the non-dimensional length (x/L) at $Re =$ 398 for IMCDCP with $s = 0.4$ mm and $h = 0.2$ mm. As demonstrated in Fig. 5(a), it can be distinctly noted that the pressure increases as the circular pin-fin diameter increases. This phenomenon occurs due to the enhancement of flow blockage effect and flow recirculation. The local pressure of IMCDCP with $d_1 = d_2 = 0.14$ mm at microchannel inlet ($x =$ 0) becomes the highest, which is increased by 16% as compared to that of IMCDCP with $d_1 = d_2 = 0.06$ mm. As shown in Fig. 5(b), the local wall temperature presents a decreasing trend with pin-fin diameter increasing, and the bigger pin-fin diameter results in the better wall temperature uniformity in the microchamber. For example, at $x/L = 0.3$, the local wall temperature of IMCDCP with $d_1 = d_2 = 0.14$ mm shows the lowest temperature, which is reduced by 3.49 K as compared to that of IMCDCP with $d_1 = d_2 = 0.06$ mm. This phenomenon can be explained by the velocity distribution and velocity vector in the microchamber, as depicted in Fig. 5(c) and (d). To show this more clearly, the vortex regions of the fluid in microchamber of IMCDCP are distinguished by red circles. It can be observed that increasing diameter leads to the intensity of vortexes behind the double circular pin-fins augmenting. This phenomenon promotes chaotic advection of fluid, thereby improving flow mixing. Furthermore, the increase in pin-fin diameter causes the fluid in the gap between two pin-fin in width direction of microchannel to accelerate, thereby thinning the boundary layer in this gap. These behaviors are beneficial to heat transfer enhancement.

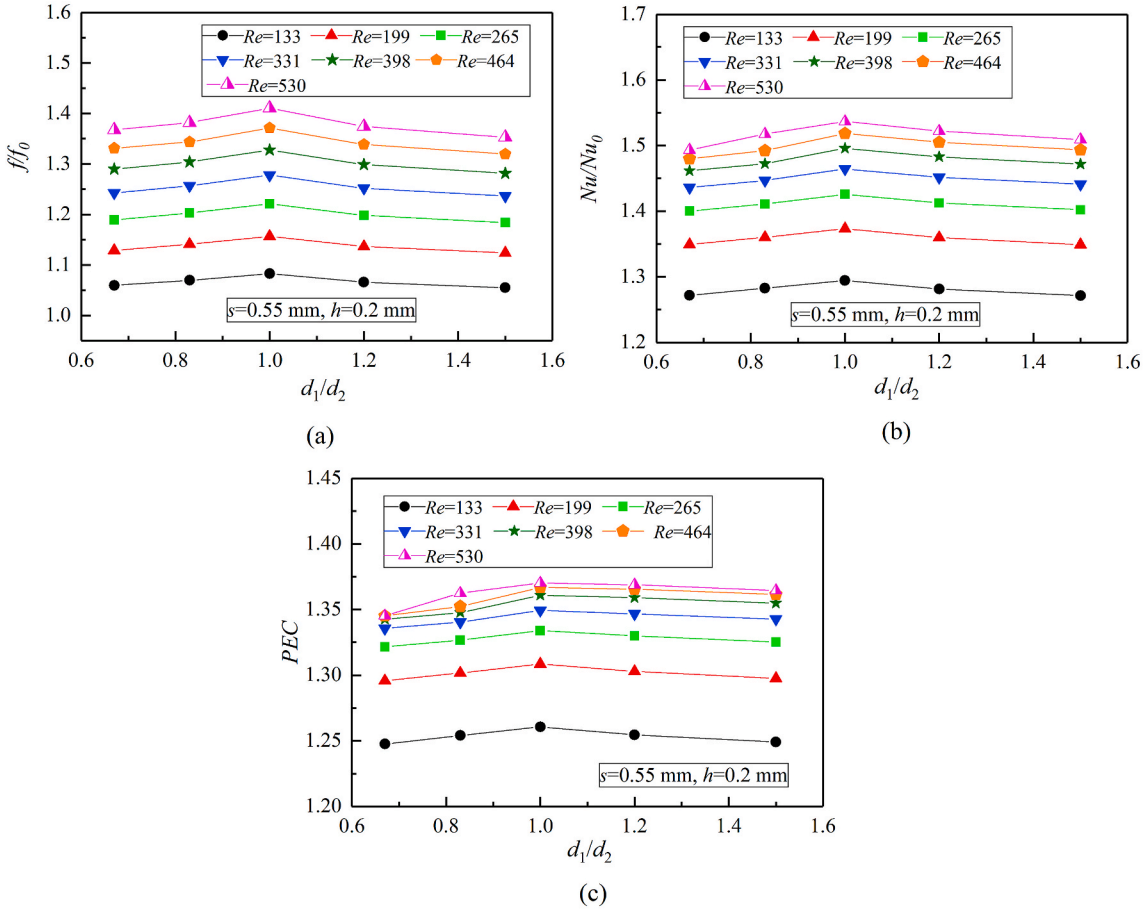

Fig. 12. Variations of (a) f/f_0, (b) Nu/Nu_0 and (c) *PEC* with combination of different pin-fin diameters for different Reynolds numbers.

3.2.3. *Effects of combination of different circular pin-fin diameters for IMCDCP*

To understand the effects of combination of different circular pin-fin diameters on local flow and heat transfer characteristics, here one of double circular pin-fins with a maximum diameter of 0.12 mm is given and the other circular pin-fin diameter is varied. Fig. 6(a) and (b) show the effects of combination of different circular pin-fin diameters (d_1 = 0.08–0.12 mm and d_2 = 0.08–0.12 mm) on local pressure (P_x) and local wall temperature ($T_{w,x}$) with the non-dimensional length (x/L) at Re = 398 for IMCDCP with s = 0.55 mm and h = 0.2 mm. As shown in Fig. 6 (a), the pressure of IMCDCP with d_1 = 0.12 mm and d_2 = 0.12 mm represents the highest value while that of IMCDCP with d_1 = 0.12 mm and d_2 = 0.08 mm represents the lowest value. However, the variation of the diameter of small pin-fin has a little effect on pressure. For example, the pressure at inlet of IMCDCP with d_1 = 0.12 mm, d_2 = 0.12 mm is increased by 2.9% as compared to IMCDCP with d_1 = 0.12 mm and d_2 = 0.08 mm. This may indicate that most of the pressure loss is caused by the maximum circular pin-fin. From Fig. 6(b), it can be observed that the wall temperature in the microchamber of IMCDCP with d_1 = 0.12 mm and d_2 = 0.08 mm as well as the IMCDCP with d_1 = 0.12 mm and d_2 = 0.1 mm (backward arrangement) are lower than that of the IMCDCP with d_1 = 0.08 mm and d_2 = 0.12 mm as well as the IMCDCP with d_1 = 0.1 mm and d_2 = 0.12 mm (forward arrangement), respectively. This means that the backward arrangement for double circular pin-fins provides better heat transfer performance as compared to forward arrangement. This reason can be explained by the velocity distribution and velocity vector, as demonstrated in Fig. 6(c) and (d). For the backward arrangement, large pin-fin diameter in upstream of microchamber can guide the fluid flow towards the laminar stagnation zone near the entrance of microchamber, thereby accelerating the heat removal. Meanwhile, it is clearly observed from Fig. 6(b) that the arrangement with $d_1 = d_2$ (IMCDCP with d_1 = 0.12 mm and d_2 = 0.12 mm) presents the lowest temperature due to the maximum heat transfer area and the strongest intensity of vortex behind the circular pin-fin. This is to say the arrangement with $d_1 = d_2$ (maximum diameter) achieves the best heat transfer enhancement rather than the backward arrangement or forward arrangement.

3.2.4. *Effects of pin-fin spacing for IMCDCP*

Fig. 7(a) and (b) display the effects of different spacings between double circular pin-fins (s = 0.25–0.85 mm) on local pressure (P_x) and local wall temperature ($T_{w,x}$) with the non-dimensional length (x/L) at Re = 398 for IMCDCP with $d_1 = d_2$ = 0.12 mm and h = 0.2 mm. In Fig. 7 (a), the pressure increases with the increase of the pin-fin spacing, but there is no appreciable change in the magnitude of pin-fin spacing on the pressure. For example, the pressure at inlet (x = 0) for IMCDCP with s = 0.85 mm is increased by 4% as compared to that with s = 0.25 mm. To clearly understand the effects of pin-fin spacing on the local pressure and local wall temperature, an enlarged view of local region of microchannel at $0.63 < x/L < 0.74$ is drawn, as shown in Fig. 7(c) and (d). From Fig. 7 (c), it can be obviously seen that the local pressure fluctuation appears in microchamber. This phenomenon can be attributed to two reasons: (1) the existent of double circular pin-fins and microchamber leads to the variation of flow area, thereby causing the pressure fluctuation due to Bernoulli effect; (2) the blockage effect caused by double circular pin-fins and the long ribs on the both sides of microchannel renders the increase in resistance loss, thereby resulting in the increasing of pressure, as demonstrated in Fig. 8(a).

In Fig. 7(b), the distribution of the local temperature shows obvious wavy fluctuation in the microchamber due to the influence of the

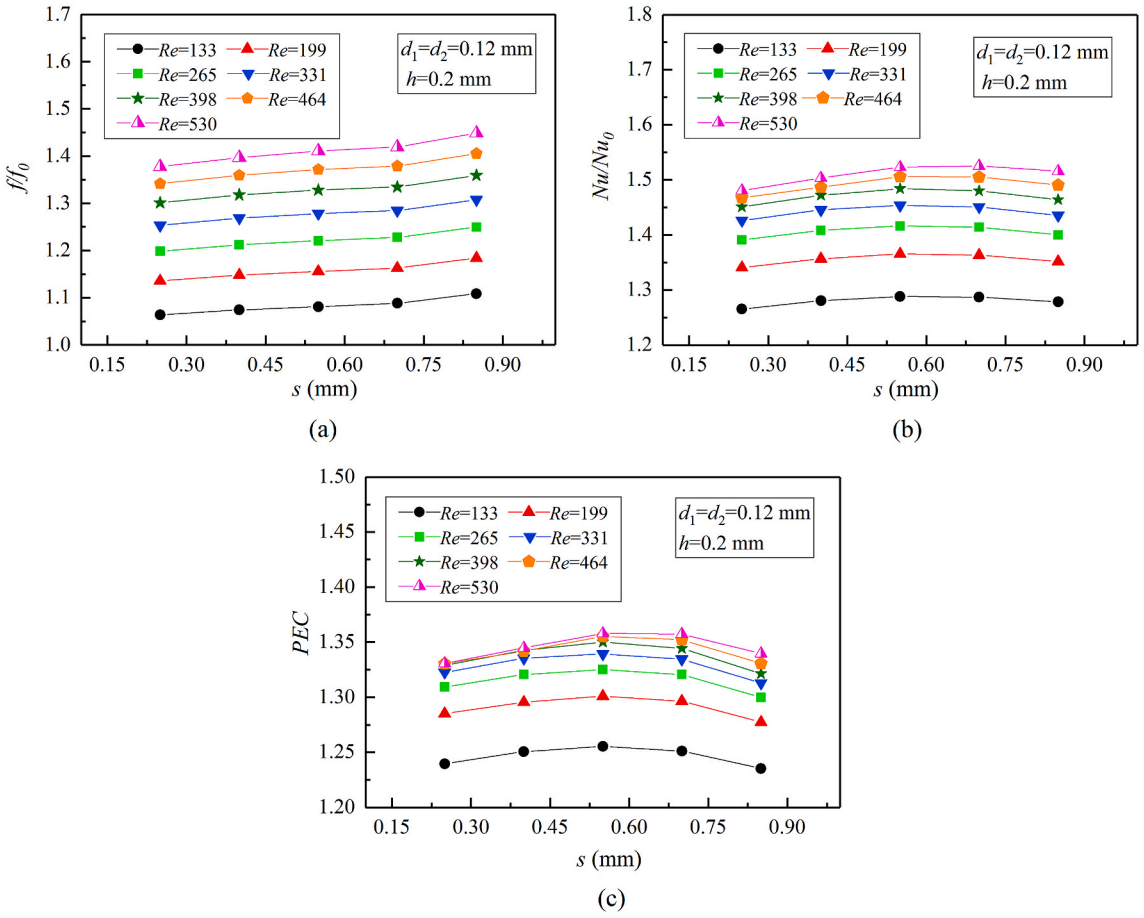

Fig. 13. Variations of (a) f/f_0, (b) Nu/Nu_0 and (c) *PEC* with pin-fin spacing for different Reynolds numbers.

combination of double circular pin-fins and microchamber. The value of local temperature near the entrance of microchamber decreases with the increase of pin-fin spacing, while it reverses in the center of the microchamber. For instance, as depicted in Fig. 7(d), the temperature at $x/L =$ 0.63 (the entrance of microchamber) of IMCDCP with $s = 0.25$ mm is increased by 1.56 K as compared to that with $s = 0.85$ mm, while the temperature at $x/L = 0.69$ (the center of microchamber) of IMCDCP with $s = 0.25$ mm is decreased by 2.03 K as compared to that with $s =$ 0.85 mm. This behavior can be explained by Fig. 8(b) and (c). The smaller pin-fin spacing causes the larger area of laminar stagnation zones to form near the entrance of microchamber, resulting in the increasing of the temperature. On the contrary, the larger pin-fin spacing reduces the area of stagnation zones near entrance of microchamber but increases the area of stagnation zones between the double circular pin-fins, thereby leading to the increase of central temperature. However, the average wall temperature (average temperature of base wall for the entire microchannel) of IMCDCP with $s = 0.85$ mm is only increased by 0.1 K than that with $s = 0.25$ mm. This indicates that the pin-fin spacing has a slight effect on average wall temperature but has a significant effect on local wall temperature. Therefore, appropriate pin-fin spacing is important for local wall temperature uniformity. Overall, the temperature of IMCDCP with $s = 0.55$ mm shows the best uniformity for wall temperature in the microchamber.

3.2.5. *Effects of pin-fin height for IMCDCP*

Fig. 9(a) and (b) present the effects of different pin-fin heights ($h =$ 0.04–0.2 mm) on local pressure (P_x) and local wall temperature ($T_{w,x}$) with the non-dimensional length (x/L) at $Re = 398$ for IMCDCP with $d_1 = d_2 = 0.12$ mm and $s = 0.55$ mm. As depicted in Fig. 9(a), the pressure at inlet ($x = 0$) increases with increasing pin-fin height. The pressure at inlet ($x = 0$) for IMCDCP with $h = 0.2$ mm is increased by 21% as compared to that with $h = 0.04$ mm. From Fig. 9(b), it can be distinctly seen that the temperatures of the most microchannels decrease with increasing of pin-fin height in microchamber except the IMCDCP with $h = 0.16$ mm. The increase of pin-fin height leads to increasing heat transfer area, thereby improving the vortex intensity and flow disturbance. This is beneficial to enhance heat transfer. It is worth noting that the IMCDCP with $h = 0.16$ mm achieves the lowest temperature in microchamber. This can be explained by the changing of the vortex structure, as shown in Fig. 9(c). With the increase of the pin-fin height, the gap between the pin-fin top and microchamber top becomes small. This will bring strong jetting effect in this gap, causing vortex structure to improve, thus strengthening the vortex intensity, thereby promoting chaotic advection and fluid mixing. It is helpful to enhancing heat transfer. However, the smaller gap also means that less fluid passes the gap, and more fluid passes the two sides of pin-fin, resulting in larger fluid velocity in the pin-fin sides. For example, when the pin-fin height is 0.2 mm, the intensities of vortexes in *xy*-plane and *yz*-plane weakens due to very low velocity behind pin-fin, as well as the intensity of vortex in *xz*-plane strengthens because of high velocity in the pin-fin sides. This suggests that the flow separation on the pin-fin sides intensifies, inducing big stagnation zone behind pin-fin, thereby rendering the cool fluid to be difficultly replenished to the heat transfer wall. It is not good for the heat removal. Consequently, above analysis indicates that there is an optimal pin-fin height to obtain the best thermal performance. In present study, the best heat transfer enhancement is obtained by IMCDCP with $h = 0.16$ mm due to the existence of good vortex structure in microchamber.

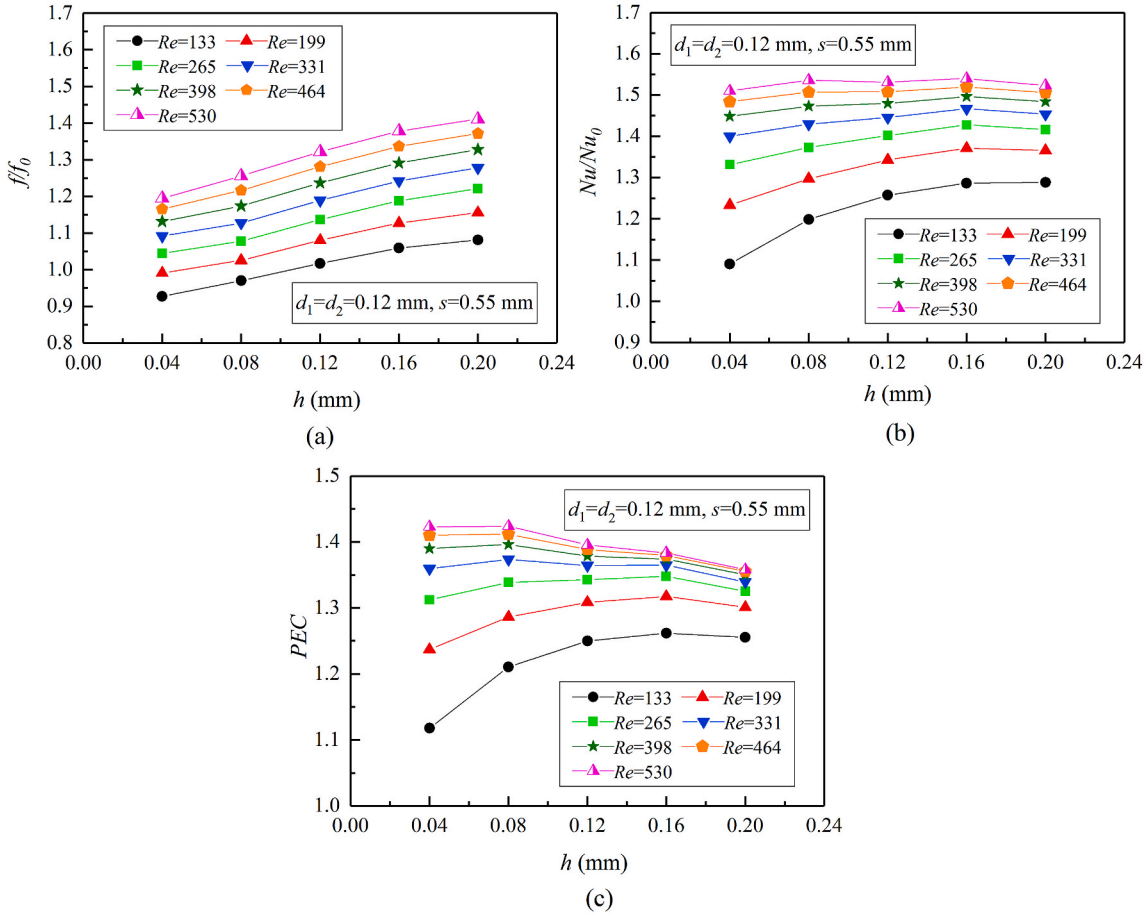

Fig. 14. Variations of (a) f/f_0, (b) Nu/Nu_0 and (c) *PEC* with pin-fin height for different Reynolds numbers.

3.3. Average flow and heat transfer performance

To analyze the effects of different microchannels on the average fluid flow and heat transfer characteristics, the average Nusselt number (*Nu*) and the average friction factor (*f*) are used to evaluate the average fluid flow and heat transfer characteristics. Hence, the effects of microchannel structure and pin-fin structural parameters on the average Nusselt number and average friction factor is investigated in detail in this section.

3.3.1. Effects of microchannel structure

Fig. 10(a) and (b) illustrate the variations of average friction factor and Nusselt number with Reynolds number for different configurations (SMC, IMC, IMCSCP and IMCDCP). From Fig. 10 (a), it can be found that the interrupted microchannels with circular pin-fin have higher friction factor than both smooth microchannel (SMC) and the interrupted microchannel without circular pin-fin (IMC). The friction factor of IMC reveals the lowest value at $Re < 265$ while that of SMC is the lowest at $Re \geq 265$. This is because the presence of microchamber increases flow area, inducing the decrease in the fluid velocity and velocity gradient, thereby reducing the friction losses. However, flow disturbance and vortex intensity will strengthen with rising *Re*, rendering the friction losses to rise. Regarding the heat transfer performance displayed in Fig. 10(b), comparing with other microchannels, the IMCDCP shows the highest average Nusselt number with a maximum value of 9.65 at $Re = 530$. This is because the double circular pin-fins in microchamber not only induce stronger vortex, as well as improve chaotic advection and fluid mixing, but also promote fluid disturbance in low fluid velocity region. Moreover, the slope of Nusselt number for IMCSCP-D decreases when $Re > 331$, which indicates that the generated vortex is obviously limited by the downstream microchannel at high Reynolds numbers.

The performance evaluation criterion is a universal criterion to evaluate the overall thermal performance of the microchannel. The variations of the performance evaluation criterion factor (*PEC*) with Reynolds number for different configurations are shown in Fig. 10(c). From Fig. 10(c), the *PEC* gradually increases with the increase of Reynolds number. The value of *PEC* in the interrupted microchannel with pin-fin is greater than that without pin-fin. This phenomenon can be attributed to stronger fluid disturbance effect on the mainstream caused by the pin-fin in the channel center. Furthermore, the IMCDCP shows higher *PEC* as compared to the IMCSCP. This suggests that the combination of double circular pin-fins and microchamber can significantly improve overall thermal performance. It is interesting to note that the *PEC* of IMCSCP-D suddenly decreases at $Re = 398$. This is because the space between the pin-fin and the microchannel is small for the pin-fin in the downstream of microchamber, limiting the vortex generation and development.

3.3.2. Effects of pin-fin diameter for IMCDCP

Fig. 11(a) and (b) present the variations of friction factor ratio (f/f_0) and heat transfer enhancement coefficient (Nu/Nu_0) with different pin-fin diameters ($d = d_1 = d_2 = 0.06$–0.14 mm) in IMCDCP with $s = 0.4$ mm and $h = 0.2$ mm for different Reynolds numbers. From Fig. 11(a), it can be observed that the value of f/f_0 increases with increasing circular pin-fin diameter at a given Reynolds number, and that also increases with the increase of Reynolds number at a given circular pin-fin diameter. The f/f_0 in IMCDCP with $d_1 = d_2 = 0.14$ mm provides the highest value ($f/f_0 = 1.50$) at $Re = 530$. As shown in Fig. 11(b), the increase of circular pin-fin diameter will increase the value of Nu/Nu_0, but the increasing rate is low. The Nu/Nu_0 in the IMCDCP with $d_1 = d_2 = 0.14$ mm achieves

the highest value ($Nu/Nu_0 = 1.53$) at $Re = 530$. Moreover, by increasing the Reynolds number, the value of Nu/Nu_0 increases at a given circular pin-fin diameter. This can be attributed to improving temperature gradient caused by the increase in vortex intensity and the effective flow mixing.

Fig. 11(c) shows the variation of performance evaluation criterion factor (*PEC*) with pin-fin diameter. It can be noted from this figure that the *PEC* gradually increases with the increase of circular pin-fin diameter at $Re < 398$, but at $Re \geq 398$, the variation of *PEC* with pin-fin diameter shows inconsistent trends. For instance, the value of *PEC* decreases slightly at first and then increases slowly with the rise of circular pin-fin diameter at $Re = 464$. However, at $Re = 530$, the value of *PEC* decreases slightly at first, then increases gradually and decreases slowly at last with the increase in pin-fin diameter. This is because for high *Re* and larger pin-fin diameter, the friction factor ratio plays a dominant role in *PEC* rather than heat transfer enhancement coefficient, as depicted in Fig. 11(a) and (b). It can be found that the IMCDCP with $d_1 = d_2 = 0.12$ mm yields the best overall thermal performance with $PEC = 1.34$ at $Re = 530$.

3.3.3. Effects of combination of different pin-fin diameters for IMCDCP

Fig. 12(a) and (b) illustrate the variations of friction factor ratio (f/f_0) and heat transfer enhancement coefficient (Nu/Nu_0) with pin-fin diameter ratio ($d_1/d_2 = 0.67$–1.5) in IMCDCP with $s = 0.55$ mm and $h = 0.2$ mm for different Reynolds numbers. From Fig. 12(a), it can be observed that the f/f_0 for IMCDCP with $d_1 = 0.12$ mm and $d_2 = 0.12$ mm ($d_1/d_2 = 1$) achieves the highest value of 1.41 at $Re = 530$. The values of f/f_0 for IMCDCP with $d_1/d_2 > 1$ (backward arrangement) are slightly lower than that with $d_1/d_2 < 1$ (forward arrangement). For example, the values of f/f_0 for IMCDCP with $d_1 = 0.12$ mm and $d_2 = 0.08$ mm ($d_1/d_2 = 1.5$) are lower than that with $d_1 = 0.08$ mm and $d_2 = 0.12$ mm ($d_1/d_2 = 0.67$). In Fig. 12(b), the values of Nu/Nu_0 for IMCDCP with $d_1 = 0.12$ mm and $d_2 = 0.12$ mm ($d_1/d_1 = 1$) achieves the highest value of 1.537 at $Re = 530$. In addition, the values of Nu/Nu_0 for IMCDCP with $d_1/d_2 > 1$ (backward arrangement) are slightly greater than that with $d_1/d_2 < 1$ (forward arrangement) at $Re \geq 199$. This indicates that pin-fin combination with backward arrangement not only enhances the heat transfer performance, but also obtains lower flow resistance as compared to that with forward arrangement. The variation of *PEC* with pin-fin diameter ratio ($d_1/d_2 = 0.67$–1.5) in IMCDCP with $s = 0.55$ mm and $h = 0.2$ mm for different Reynolds numbers is presented in Fig. 12(c). From Fig. 12 (c), the highest *PEC* is achieved by IMCDCP with $d_1 = 0.12$ mm and $d_2 = 0.12$ mm ($d_1/d_2 = 1$) at the whole range of studied Reynolds number.

3.3.4. Effects of pin-fin spacing for IMCDCP

Fig. 13(a) and (b) show variations of friction factor ratio (f/f_0) and heat transfer enhancement coefficient (Nu/Nu_0) with pin-fin spacing ($s = 0.25$–0.85 mm) in IMCDCP with $d_1 = d_2 = 0.12$ mm and $h = 0.2$ mm. In Fig. 13(a), a slight increase of f/f_0 has been noted with the increase in pin-fin spacing. This is because the increase in pin-fin spacing strengthens flow blockage effect for the regions of entrance and exit in microchamber, thereby causing the increasing of friction loss. Therefore, the IMCDCP with $s = 0.85$ mm achieves the highest friction factor with $f/f_0 = 1.45$ at $Re = 530$. In Fig. 13(b), it is clearly seen that with the increase of circular pin-fin spacing, the Nu/Nu_0 gradually increases at first, and then decreases. The main reason of this phenomenon can be explained by the fact that, for small pin-fin spacing, the development of vortex caused by pin-fin in the upstream is interrupted due to the existence of pin-fin in the downstream. Also, it cannot impact the stagnation zone well near the entrance of microchamber because this pin-fin is far from the entrance of microchamber. The large pin-fin spacing can further induce the fluid to flow towards the stagnation zone in microchamber, but the intensity of vortex caused by the pin-fin in the downstream will weaken. Therefore, the IMCDCP with $s = 0.55$ mm shows the highest Nu/Nu_0 as $Re \leq 464$. Moreover, it is noticed that the Nu/Nu_0 of IMCDCP with $s = 0.7$ mm is higher than that of other microchannels at $Re = 530$, while the IMCDCP with $s = 0.25$ mm shows the lowest value of Nu/Nu_0 within the all *Re*. In addition, the Nu/Nu_0 of IMCDCP with $s = 0.85$ mm is lower than that of IMCDCP with $s = 0.4$ mm at $Re < 464$. However, at $Re \geq 464$, the IMCDCP with $s = 0.85$ mm obtains a higher Nu/Nu_0 than IMCDCP with $s = 0.4$ mm. This is because the higher velocity promotes the intensity of vortex between two pin-fins, thereby enhancing heat transfer, especially for larger pin-fin spacing.

The variation of *PEC* with pin-fin spacing is presented in Fig. 13(c). It is found that the IMCDCP with $s = 0.55$ mm provides the highest *PEC* of 1.36 at $Re = 530$, while the one with $s = 0.85$ mm provides the lowest *PEC* of 1.235 at $Re = 133$. As $Re > 265$, there is a slight effect on *PEC* for small pin-fin spacing as compared to the large pin-fin spacing. Moreover, the *PEC* of IMCDCP with $s = 0.85$ mm is the lowest at $Re < 464$, but at $Re \geq 464$, the *PEC* of IMCDCP with $s = 0.85$ mm is higher than that with $s = 0.25$ mm. This possibly means that the larger pin-fin spacing will reach a better overall thermal performance than the smaller pin-fin spacing at high *Re,* but this trend is contrary at low *Re.*

3.3.5. Effects of pin-fin height for IMCDCP

Fig. 14(a) and (b) describe the variations of friction factor ratio (f/f_0) and heat transfer enhancement coefficient (Nu/Nu_0) with pin-fin height ($h = 0.04$–0.2 mm) in IMCDCP with $d_1 = d_2 = 0.12$ mm and $s = 0.55$ mm. In Fig. 14(a), the value of f/f_0 increases with increasing pin-fin height. The value of f/f_0 in IMCDCP with $h = 0.2$ mm is the highest ($f/f_0 = 1.42$). From Fig. 14(b), it is observed that Nu/Nu_0 presents an increasing trend at first and then a decreasing trend as pin-fin height increasing under the most Reynolds numbers, but there is a slight variation in the magnitude of Nu/Nu_0 with pin-fin height when $Re > 331$. This is attributed to the increment in surface area of heat transfer and the vortex intensifying, resulting in the heat transfer enhancement. However, high fluid velocity will enhance the effect of the flow separation on the pin-fin sides, which is bad for heat transfer enhancement, especially for higher pin-fin height. It can be noted that the best heat transfer performance is obtained by IMCDCP with $h = 0.16$ mm, and the maximum value of Nu/Nu_0 reaches 1.54.

The variation of *PEC* with pin-fin height is presented in Fig. 14(c). It can be seen that the curve of *PEC* for all Reynolds numbers shows an increasing trend at first and then a decreasing trend with the increase of pin-fin height. However, the maximum value of *PEC* shifts leftwards with the increase of Reynolds number. For example, the maximum *PEC* in IMCDCP with $h = 0.16$ mm is obtained when $Re \leq 265$, but when $Re > 265$, that in IMCDCP with $h = 0.08$ mm shows the maximum value. One can also observe from this figure that the value of *PEC* at $Re > 265$ and $h > 0.08$ mm decreases rapidly with the pin-fin height increasing. This is because the Nu/Nu_0 has a slight variation with pin-fin height increasing at high Reynolds number, but the f/f_0 increases rapidly with the increase of pin-fin height, as shown in Fig. 14(a) and (b). In addition, it can be concluded that the pin-fin with higher height achieves better overall thermal performance at low Reynolds number. However, at high Reynolds number, the pin-fin with lower height provides better overall thermal performance. This means that the optimum height of pin-fin for the best overall thermal performance depends on Reynolds number. In other word, the pin-fin height should be decreased at high Reynolds number or that should be increased at low Reynolds number to obtain the best overall thermal performance. Furthermore, the IMCDCP with $h = 0.08$ mm yields the maximum *PEC* of 1.42 at $Re = 530$.

4. Conclusions

In the present work, the interrupted microchannel with double circular pin-fins in each microchamber (IMCDCP) is designed. The effects of geometric parameters of pin-fin on local fluid flow and heat transfer characteristics at Reynolds number (*Re*) of 398 and average fluid flow and heat transfer characteristics with *Re* ranging from 133 to 530 in IMCDCP are studied numerically. The geometric parameters include the

diameter (d_1) of pin-fin in upstream of microchamber, the diameter (d_2) of pin-fin in downstream of microchamber, the spacing (s) between double pin-fins, and the height (h) of pin-fin. In addition, these results obtained by IMCDCP are compared with those obtained by the smooth microchannel (SMC), the interrupted microchannel (IMC) and the interrupted microchannel with single circular pin-fin in each microchamber (IMCSCP). The following conclusions can be drawn:

(1) Comparing with the SMC, the IMC and the IMCSCP, the IMCDCP not only archives lower local wall temperature and better wall temperature uniformity, but also provides the excellent heat transfer enhancement and the superior overall thermal performance.
(2) Increasing the pin-fin diameter in microchamber will reduce the local wall temperature and improve the heat transfer enhancement, but increase the pressure drop and give rise to the larger friction losses. In addition, the analysis result of combination of different pin-fin diameters shows that the pin-fin with the largest diameter plays a dominant role in the magnitude of the pressure. The arrangement of double circular pin-fins with $d_1 = d_2$ provides the best heat transfer and overall thermal performance, as compared to that with $d_1 > d_2$ or $d_1 < d_2$.
(3) The pin-fin spacing in microchamber has a slight effect on the pressure drop between inlet and outlet and average wall temperature, but it plays an importance role in local wall temperature. This indicates that the appropriate pin-fin spacing is significant for wall temperature uniformity. In this study, the IMCDCP with s = 0.55 mm shows the best wall temperature uniformity in the microchamber. Comparing with other pin-fin spacings, the IMCDCP with $s = 0.55$ mm ($d_1 = d_2 = 0.12$ mm, $h = 0.2$ mm) shows the highest Nu/Nu_0 at $Re \leq 464$ and the best overall thermal performance at studied range of Re.
(4) The proper pin-fin height in microchamber not only enhances the heat transfer, but also improves the overall thermal performance. The results suggest that the IMCDCP with $h = 0.16$ mm ($d_1 = d_2 = 0.12$ mm, $s = 0.55$ mm) achieves the lowest local wall temperature in microchamber. Meanwhile, this IMCDCP provides the highest heat transfer enhancement, which the maximum Nu/Nu_0 yields 1.54 at $Re = 530$. Under the range of studied Reynolds number, the best overall thermal performance of the IMCDR with $h = 0.08$ mm ($d_1 = d_2 = 0.12$ mm, s = 0.55 mm) yields the maximum PEC of 1.42 at $Re = 530$.

The designed IMCDCP can efficiently improve the overall thermal performance, as well as obtain low wall temperature and good wall temperature uniformity. This suggests that the IMCDCP has the potential to be a nice cooling device for applications involving hot spots mitigation in the electronic devices or fuel cell bipolar plate. Furthermore, to analyze the fluid flow and heat transfer characteristics for IMCDCP in detail from the viewpoint of the second law of thermodynamics, the investigation of entropy generation due to flow and heat transfer in the IMCDCP will be carried out in the future study.

Declaration of competing interest

The authors declared that there is no conflict of interest.

Data availability

Data will be made available on request.

Acknowledgments

This research has been supported by National Natural Science Foundation of China (No. 21666005) and the Dean Project of Guangxi Key Laboratory of Petrochemical Resource Processing and Process Intensification Technology (No. 2019Z012).

References

[1] W. Ling, W. Zhou, C. Liu, F. Zhou, D. Yuan, J. Huang, Structure and geometric dimension optimization of interlaced microchannel for heat transfer performance enhancement, Appl. Therm. Eng. 170 (2020) 115011.
[2] D.B. Tuckerman, R.F.W. Pease, High-performance heat sinking for VLSI, IEEE Electron. Device Lett. 2 (1981) 126–129.
[3] Z. Feng, X. Ai, P. Wu, Q. Lin, Z. Huang, Experimental investigation of laminar flow and heat transfer characteristics in square minichannels with twisted tapes, Int. J. Heat Mass Tran. 158 (2020) 119947.
[4] D. Jing, L. He, Numerical studies on the hydraulic and thermal performances of microchannels with different cross-sectional shapes, Int. J. Heat Mass Tran. 143 (2019) 118604.
[5] E. Bayrak, A.B. Olcay, M.F. Serincan, Numerical investigation of the effects of geometric structure of microchannel heat sink on flow characteristics and heat transfer performance, Int. J. Therm. Sci. 135 (2019) 589–600.
[6] M. Jeong, M.Y. Ha, Y.G. Park, Numerical investigation of heat transfer enhancement in a dimpled cooling channel with different angles of the vortex generator, Int. J. Heat Mass Tran. 144 (2019) 118644.
[7] G.V. Kewalramani, G. Hedau, S.K. Saha, A. Agrawal, Study of laminar single phase frictional factor and Nusselt number in In-line micro pin-fin heat sink for electronic cooling applications, Int. J. Heat Mass Tran. 138 (2019) 796–808.
[8] V.A. Martínez, D.A. Vasco, C.M. García-Herrera, R. Ortega-Aguilera, Numerical study of TiO_2-based nanofluids flow in microchannel heat sink: effect of the Reynolds number and the microchannel height, Appl. Therm. Eng. 161 (2019) 114130.
[9] M. Ding, C. Liu, Z. Rao, Experimental investigation on heat transfer characteristic of TiO_2-H_2O nanofluid in microchannel for thermal energy storage, Appl. Therm. Eng. 160 (2019) 114024.
[10] X. Lin, S. Mo, B. Mo, L. Jia, Y. Chen, Z. Cheng, Thermal management of high-power LED based on thermoelectric cooler and nanofluid-cooled microchannel heat sink, Appl. Therm. Eng. 172 (2020) 115165.
[11] M. Bahiraei, M. Jamshidmofid, M. Goodarzi, Efficacy of a hybrid nanofluid in a new microchannel heat sink equipped with both secondary channels and ribs, J. Mol. Liq. 273 (2019) 88–98.
[12] Y. Yue, S.K. Mohammadian, Y. Zhang, Analysis of performances of a manifold microchannel heat sink with nanofluids, Int. J. Therm. Sci. 89 (2015) 305–313.
[13] M. Khoshvaght-Aliabadi, S.M. Hassani, S.H. Mazloumi, Enhancement of laminar forced convection cooling in wavy heat sink with rectangular ribs and Al_2O_3/water nanofluids, Exp. Therm. Fluid Sci. 89 (2017) 199–210.
[14] O.A. Alawi, N.A.C. Sidik, H.A. Mohammed, A comprehensive review of fundamentals, preparation and applications of nanorefrigerants, Int. Commun. Heat Mass Tran. 54 (2014) 81–95.
[15] M. Khoshvaght-Aliabadi, M. Sahamiyan, M. Hesampour, O. Sartipzadeh, Experimental study on cooling performance of sinusoidal-wavy minichannel heat sink, Appl. Therm. Eng. 92 (2016) 50–61.
[16] M. Pan, H. Wang, Y. Zhong, M. Hu, X. Zhou, G. Dong, P. Huang, Experimental investigation of the heat transfer performance of microchannel heat exchangers with fan-shaped cavities, Int. J. Heat Mass Tran. 134 (2019) 1199–1208.
[17] L. Chai, G. Xia, L. Wang, M. Zhou, Z. Cui, Heat transfer enhancement in microchannel heat sink with periodic expansion-constriction cross-sections, Int. J. Heat Mass Tran. 62 (2013) 741–751.
[18] Z. Wan, Q. Lin, X. Wang, Y. Tang, Flow characteristics and heat transfer performance of half-corrugated microchannels, Appl. Therm. Eng. 123 (2017) 1140–1151.
[19] D. Yuan, W. Zhou, T. Fu, C. Liu, Experimental and numerical investigation of heat and mass transfer in non-uniform wavy microchannels, Int. J. Heat Mass Tran. 152 (2020) 106320.
[20] X. Liu, H. Zhang, C. Zhu, F. Wang, Z. Li, Effects of structural parameters on fluid flow and heat transfer in a serpentine microchannel with fan-shaped reentrant cavities, Appl. Therm. Eng. 151 (2019) 406–416.
[21] N. Raja Kuppusamy, R. Saidur, N.N.N. Ghazali, H.A. Mohammed, Numerical study of thermal enhancement in micro channel heat sink with secondary flow, Int. J. Heat Mass Tran. 78 (2014) 216–223.
[22] X. Shi, S. Li, Y. Mu, B. Yin, Geometry parameters optimization for a microchannel heat sink with secondary flow channel, Int. Commun. Heat Mass Tran. 104 (2019) 89–100.
[23] M. Yang, B.-Y. Cao, Numerical study on flow and heat transfer of a hybrid microchannel cooling scheme using manifold arrangement and secondary channels, Appl. Therm. Eng. 159 (2019) 113896.
[24] L. Chai, L. Wang, X. Bai, Thermohydraulic performance of microchannel heat sink with triangular ribs on sidewalls-Part 1: local fluid flow and heat transfer characteristics, Int. J. Heat Mass Tran. 127 (2018) 1124–1137.
[25] Y.K. Prajapati, Influence of fin height on heat transfer and fluid flow characteristics of rectangular microchannel heat sink, Int. J. Heat Mass Tran. 137 (2019) 1041–1052.
[26] G. Wang, T. Chen, M. Tian, G. Ding, Fluid and heat transfer characteristics of microchannel heat sink with truncated pin-fin on sidewall, Int. J. Heat Mass Tran. 148 (2020) 119142.
[27] J. Li, Z. Zhu, L. Zhao, H. Peng, Experimental investigation of the heat transfer and flow characteristics of microchannels with microribs, Int. J. Heat Mass Tran. 143 (2019) 118482.

[28] Y. Jia, G. Xia, Y. Li, D. Ma, B. Cai, Heat transfer and fluid flow characteristics of combined microchannel with cone-shaped micro pin fins, Int. Commun. Heat Mass Tran. 92 (2018) 78–89.
[29] Y. Wang, B. Zhou, Z. Liu, Z. Tu, W. Liu, Numerical study and performance analyses of the mini-channel with discrete double-inclined ribs, Int. J. Heat Mass Tran. 78 (2014) 498–505.
[30] E. Hosseinirad, M. Khoshvaght-Aliabadi, F. Hormozi, Evaluation of heat transfer and pressure drop in a mini-channel using transverse rectangular vortex-generators with various non-uniform heights, Appl. Therm. Eng. 161 (2019) 114196.
[31] D.D. Ma, G.D. Xia, W. Wang, Y.T. Jia, Y.C. Yang, Study on thermal performance of microchannel heat sink with periodic jetting and throttling structures in sidewalls, Appl. Therm. Eng. 158 (2019) 113764.
[32] G. Wang, N. Qian, G. Ding, Heat transfer enhancement in microchannel heat sink with bidirectional rib, Int. J. Heat Mass Tran. 136 (2019) 597–609.
[33] Wan Mohd Arif Aziz Japar, Nor Azwadi Che Sidik, Shabudin Mat, A overall study on heat transfer enhancement in microchannel heat sink with secondary channel, Int. Commun. Heat Mass Tran. 99 (2018) 62–81.
[34] I.A. Ghani, N. Kamaruzaman, N.A.C. Sidik, Heat transfer augmentation in a microchannel heat sink with sinusoidal cavities and rectangular ribs, Int. J. Heat Mass Tran. 108 (2017), 1969–1981.
[35] Y.F. Li, G.D. Xia, D.D. Ma, Y.T. Jia, J. Wang, Characteristics of laminar flow and heat transfer in microchannel heat sink with triangular cavities and rectangular ribs, Int. J. Heat Mass Tran. 98 (2016) 17–28.
[36] I.A. Ghani, N.A.C. Sidik, R. Mamat, G. Najafi, T.L. Ken, Y. Asako, W.M.A.A. Japar, Heat transfer enhancement in microchannel heat sink using hybrid technique of ribs and secondary channels, Int. J. Heat Mass Tran. 114 (2017) 640–655.
[37] A. Datta, V. Sharma, D. Sanyal, P. Das, A conjugate heat transfer analysis of performance for rectangular microchannel with trapezoidal cavities and ribs, Int. J. Therm. Sci. 138 (2019) 425–446.
[38] R. A, S. Chakraborty, Effect of micro–structures in a microchannel heat sink - a comprehensive study, Int. J. Heat Mass Tran. 154 (2020) 119617.
[39] M.A. Alfellag, H.E. Ahmed, O.T. Fadhil, A. Sh Kherbeet, Optimal hydrothermal design of microchannel heat sink using trapezoidal cavities and solid/slotted oval pins, Appl. Therm. Eng. 158 (2019) 113765.
[40] L. Chai, G. Xia, M. Zhou, J. Li, J. Qi, Optimum thermal design of interrupted microchannel heat sink with rectangular ribs in the transverse microchambers, Appl. Therm. Eng. 51 (1–2) (2013) 880–889.